International Journal of Architectural, Civil and Construction Sciences
ISSN: 2415-1734
Vol:6, No:5, 2012

Numerical Modeling of Steel-Composite Hybrid Tubes Subject to Static and Dynamic Loading

Y. S. Tai, M. Y. Huang, and H. T. Hu

***Abstract*—**The commercial finite element program LS-DYNA was employed to evaluate the response and energy absorbing capacity of cylindrical metal tubes that are externally wrapped with composite. The effects of composite wall thickness, loading conditions and fiber ply orientation were examined. The results demonstrate that a wrapped composite can be utilized effectively to enhance the crushing characteristics and energy absorbing capacity of the tubes. Increasing the thickness of the composite increases the mean force and the specific energy absorption under both static and dynamic crushing. The ply pattern affects the energy absorption capacity and the failure mode of the metal tube and the composite material property is also significant in determining energy absorption efficiency.

***Keywords*—**fiber-reinforced metal tubes, energy absorption, axial crushing, impact loading.

I. Introduction

NUMEROUS practical engineering systems must absorb various amounts of energy during impact events. In recently years, fiber composite materials have been increasingly used in the development of advanced metal shell structures. Owing to their superior strength-to-weight ratio, hybrid structures are excellent for energy absorption and have been extensively used in such engineering structures as automobiles, aircraft, military facilities, bridge structures and others. As a result, several researchers have recently addressed metal tubes that wrapped with a fiber-reinforced plastic composite. Various experimental and theoretical studies of the behaviors of different material and hybrid tubes have been carried out [1, 2, 3, 4, 5, 6, 7, 8, 9, 10, 11, 12, 13, 14, 15, 16].

The theoretical model developed by Alexander (1960) for calculating the average crushing force of a cylindrical tube under static axial crush is well known. Bambach (2010) studied the axial capacity and crushing of thin-walled metal, fiber-epoxy and composite metal-fiber tubes and utilized a photogrammetry system to determine the buckling behavior. Furthermore, when combined with previous theories, a general design procedure for metal, fiber-epoxy and metal-fiber tubes has been demonstrated. Based on Alexander's classical solution, Hanefi and Wierzbicki (1996) proposed a simplified analytical model of the static crushing of externally reinforced metal tubes, which agrees closely with experimental data.

Hage *et al.* (2004) developed a finite element model based on modified Chang-Chang failure criteria to elucidate the quasi-static axial crush behavior of square aluminum-composite hybrid tubes.

They also explored the effects of adhesion, friction between the aluminum tubes overwrapping with composite and verified their numerical model using experimental data.

Y. S. Tai is with the Department of Civil Engineering, ROC Military Academy, Taiwan, ROC (phone: 886-7-7456290; e-mail: ystai@mail.cma.edu.tw).

M. Y. Huang, and H. T. Hu is with the Department of Civil Engineering, National Cheng Kung University, Taiwan, ROC.

Han *et al.* (2007) numerically studied hybrid composite unidirectional pultruded tubes that are over-wrapped with ±45° braided fiber-reinforced plastic, to elucidate their crushing behavior and energy absorbing capacity. Parametric investigations of the effects of the length of the tube, the thickness and type of braid, and the loading conditions on the crushing behavior of the tubes have been examined. Huang and Wang (2009) proposed a two-layer finite element model of the static axial collapse of carbon-reinforced composite tubes. The numerical simulation can effectively model the bevel trigger, representing the energy absorption characteristics and crushing failure mode of the composite specimens. Kadi (2008) use the artificial neural networks (ANN) technique to predict the crushing behavior and energy absorption characteristics of composite elliptical tubes. He considers the effects of parameters such as network architecture, number of hidden layers and number of neurons per hidden layer. To compare with actual experimental results, the predictions are shown to be in good agreement. Mamalis *et al.* (2006) adopted LS-DYNA3D to perform a numerical simulation investigates the crushing response of square carbon FRP tubes subjected to static axial compression and impact testing. Factors include length, wall thickness , laminate stacking sequence and fiber volume content are examined. To regard the main crushing characteristics of the peak load, crash energy absorption and the overall crushing response, the experimental results are performed to validate the simulations and good correlation is achieved.

Furthermore, on the property of metal material, Marais (2004) *et al.* revealed that stress level, and prior work hardening, heat treatment condition and microstructure of these earlier tests, as these variables affect the Cowper-Symonds constitutive equation constants. In view of this, the metal stress-strain curves of different strain rate used in the numerical simulation were obtained from tensile tests by Hopkinson Split Bar in this study.

Most previous studies of the crushing behavior of fiber-reinforced metal tubes were purely experimental. In this investigation, numerical simulations are carried out using the explicit non-linear finite element commercial software LS-DYNA and the results are compared with theoretical predictions to study how to establish an effective model for predicting the energy absorption behavior of hybrid tubes. The purpose is to develop a numerical method for evaluating the static and dynamic behavior of fiber-reinforced metal tubes under axial load. The effects of composite thickness, stacking orientations and material property of composite are also emphasized.

II. Analytical Model

Based on Alexander's model of metal tubes, Hanefi and Wierzbicki (1996) proposed a simplified analytical model of the static compression of externally composite-reinforced metal

tubes, with an angle of orientation of the overwrap from the tube axis of 0° (Fig.1). Consider the crushing mechanism of five stationary plastic hinges that produces a folding that is composed of four elements of equal lengths. According to the model, when the composite walls are under tension at the outward fold, the glass fibers do not contribute to the resistance of the composite material. Accordingly, at hinge lines 2 and 4, the contribution of the composite wall is negligible, and the resisting bending moment of the metal walls is given by

$$M_0^{(2)} = M_0^{(4)} = \frac{\sigma_0 t_m^2}{4} \tag{1}$$

where σ_0 and t_m are the yield strength and wall thickness of metal, respectively. Similarly, at hinge line 3, when the composite walls are under compression at the inward fold, the bending moment of the bi-material section is given by Eq. (2). The mean of the bending moments calculated using Eqs. (1) and (2) yields Eq. (3) .

$$M_0^{(3)} = \frac{\sigma_0 t_m^2}{4}[1+2(\frac{\sigma_{cr}}{\sigma_0})(\frac{t_c}{t_m})+2(\frac{\sigma_{cr}}{\sigma_0})(\frac{t_c}{t_m})^2-(\frac{\sigma_{cr}}{\sigma_0})^2(\frac{t_c}{t_m})^2] \tag{2}$$

$$M_0 = C\frac{\sigma_0 t_m^2}{4} \tag{3}$$

$$C = \frac{1}{2}[2+2(\frac{\sigma_{cr}}{\sigma_0})(\frac{t_c}{t_m})+2(\frac{\sigma_{cr}}{\sigma_0})(\frac{t_c}{t_m})^2-(\frac{\sigma_{cr}}{\sigma_0})^2(\frac{t_c}{t_m})^2] \tag{4}$$

σ_{cr} is the ultimate stress of composite in compression perpendicular to fiber direction, t_c is the wall thickness of composite. Furthermore, to satisfy the Tresca yield criteria, the contribution of the metal shell to the membrane energy and the bending energy that is dissipated in the wall of the hybrid tube must be

$$W_b = 2\pi^2 aC\sigma_0 t_m^2 \tag{5}$$

$$W_m = r\pi\sigma_0 t_m H^2 \tag{6}$$

where a is initial radius of tube and H is the hinge length.

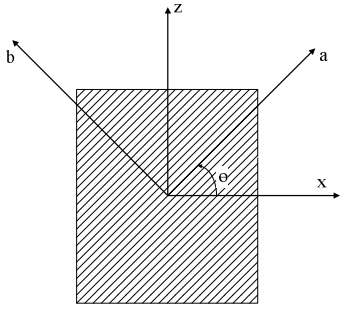

Fig. 1 Material coordinate system for a fiber reinforced lamina in which a is the fiber direction and b is the transverse direction

During the formation of a fold, when the composite is under tension, the contribution of the composite to the membrane energy consists of two parts with the interface between the fractured and unfractured of the composite.

Simplification yields the energy absorbed by the composite reinforcement in tension and compression, given by Eqs. (7) and (8), respectively.

$$(W_c)_{ten} = 2\pi a t_c E_c[\int_0^{w_{ct}}(\frac{s}{a})^2 ds + \int_{w_{ct}}^{H} {\varepsilon_{ct}}^2 ds] \tag{7}$$

$$(W_c)_{com} = 2\pi a t_c \int_0^{2H} \sigma_{cf}\frac{s}{a} ds \tag{8}$$

Accordingly,

$$W_c = (W_c)_{ten} + (W_c)_{com} = 2\pi t_c H(H\sigma_{cf} + aE_c{\varepsilon_{ct}}^2) \tag{9}$$

where σ_{cf} and ε_{ct} are, respectively, the ultimate stress of composite in compression in fiber direction and strain limits of composite in tension in fiber direction, E_c is Young's modulus of composite in tension in fiber direction, w_{ct} is the length of unfractured composite parts and the interface between the fractured and unfractured parts is denoted by $s = w_{ct}$. The external work equals the internal energy dissipated for a given crushing distance. Abramowicz (1983) developed an approximate expression for the actual compression length of metal columns and determined an effective crushing length. Finally, the crushing load P_m is obtained:

$$P_m = \frac{1}{3.44H-2t}(2\pi^2 a\sigma_0 C{t_m}^2 + 4\pi t\sigma_{eq}H^2 + 2\pi a t_c E_c{\varepsilon_{ct}}^2 H) \tag{10}$$

$$\sigma_{eq} = (\sigma_0 t_m + \frac{1}{2}\sigma_{cf}t_c)/t \tag{11}$$

However, considering the mechanism of crumpling of hybrid tubes that was proposed by Hanefi and Wierzbicki (1996), Wang (2002) considered the deformation of both radial inward and outward folds. In calculating the bending energy, they assumed that the metal tubes obeyed the Von Mises yield criterion and considered the resistance of the fiber-reinforced layer to tensile bending deformation. Hence, they derived the three contributory terms and a formula for P_m that differed from that of Hanefi and Wierzbicki (1996), as follows.

$$W_b = \frac{4}{\sqrt{3}}\pi^2 a\sigma_0 t_m^2 C_0 + \frac{2}{\sqrt{3}}\pi\sigma_0 {t_m}^2 HC_1 \tag{12}$$

$$C_0 = 1+(\frac{\sigma_{cxc}+\sigma_{cxt}}{\sigma_0})(\frac{t_c}{t_m})+(\frac{\sigma_{cxc}+\sigma_{cxt}}{\sigma_0})(\frac{t_c}{t_m})^2 - 0.5(\frac{{\sigma_{cxc}}^2+{\sigma_{cxt}}^2}{{\sigma_0}^2})^2(\frac{t_c}{t_m})^2 \tag{13}$$

$$C_1 = (\frac{\sigma_{cxc}+\sigma_{cxt}}{\sigma_0})(\frac{t_c}{t_m})+(\frac{\sigma_{cxt}+\sigma_{cxc}}{\sigma_0})(\frac{t_c}{t_m})^2 - 0.5(\frac{{\sigma_{cxt}}^2-{\sigma_{cxc}}^2}{{\sigma_0}^2})^2(\frac{t_c}{t_m})^2 \tag{14}$$

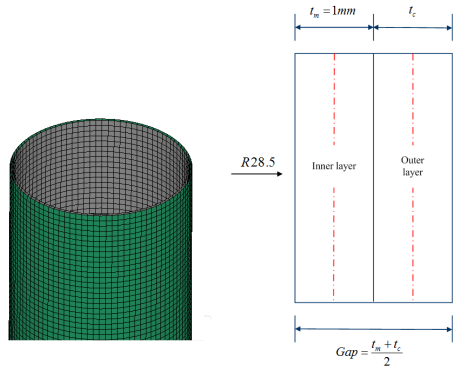

(a) modelling of the tube (b)Cross section of compound tube wall

Fig. 2 Finite element model of steel-composite compound tube

$$W_m = 2\pi\sigma_0 t_m H^2 + 2\pi H^2 t_m \sigma_0$$

$$W_c = \frac{2}{3}\pi a^2 t_c \sigma_{ct} \varepsilon_{ct}^{\ 2} + 2\pi H^2 t_c \sigma_{cc} \quad (16)$$

$$P_m = \frac{1}{3.44H - 2t}(4\pi t \sigma_{eq} H^2 + \frac{2}{\sqrt{3}}\pi\sigma_0 t_m^{\ 2} C_1 H + \frac{4}{\sqrt{3}} a\pi^2 \sigma_0 t_m^{\ 2} C_0 + \frac{2}{3}\pi a^2 t_c \sigma_{ct} \varepsilon_{ct}^{\ 2}) \quad (17)$$

where σ_{cxc} and σ_{cxt} are axial compressive strength and axial tensile strength of the fiber-reinforced layer, respectively, σ_{cc} is critical stress in the fiber direction subjected to compression and σ_{ct} is critical stress in the fiber direction subjected to tension.

III. Numerical Simulations

A. Description of Analysis Model

All numerical simulations were conducted using the commercial finite element program LS-DYNA (2006). Steel-composite hybrid tubes were geometrically modeled as two-layer cylindrical shells, as displayed in Fig 2. The dimensions of the extruded metal tube in all of the models were L=170mm, D=58mm and t=1.0mm, and composite wall thicknesses of 0.5mm, 0.8mm and 1.0mm were considered.

Both steel and composite tubes were modeled using Belytschko-Tsay four-node shell elements. The steel and composite mid-planes were separated by a small gap that equaled the average thickness of the two walls (Fig.2) and the stiffness-type hourglass control model was adopted to eliminate the zero-energy modes. The steel tube was modeled using three integration points through the thickness and one integration point in the element plane. Additionally, the different layers with certain stacking orientations were defined using integration points of the composite each of which represented one stacking lay-up.

Due to the fact that the explicit time integration method is only conditionally stable, and therefore, in general, very small time increments have to be used. One of the ways of achieving a quasi-static process by using the explicit dynamic procedure is to scale up the mass, while keeping velocity very low.

Scaling up the mass results in a large time step, therefore reducing the number of time step increments for such a low loading rate. A simulation was carried out using a whole model because of uncertainty in the destruction pattern. In all simulations of axial crushing, the bottom end of the tube was assumed to be built-in and is constrained in all degrees of freedom. The upper end was free and compressed by rigid loading plate that moved at a downward initial velocity.

In the quasi-static and dynamic crushing simulations of interaction between steel and composite walls, the three contact algorithms were applied to avoid interpenetration during the movement and progressive folding. To simulate the interaction between the steel and the composite overwrap, the friction coefficient between all of the contact surfaces was set to 0.2. Three different maximum normal and shear failure forces were considered for the investigation of bond failure limit. The values selected were 100N, 250N and 750N to represent weak bond, medium strength bond and strong bond, respectively. Fig. 3 shows the force-deformation for the three cases. It is clearly seen that the crushing deformation with 100N and 300N were similar and the 750N model showed a different deformation. Furthermore, to compare the peak force of the 100N was close to predict value in Eqs. (10) and (17). Based on these observations, it was decided that the 100N bond failure limit was selected for other numerical simulations.

$$(\frac{f_n}{NFLF})^2 + (\frac{f_s}{SFLF})^2 \geq 1.0 \quad (18)$$

where f_n, f_s ,NFLF and SFLF are normal force at the interface, shear force at the interface, maximum normal force at bond failure and maximum shear force at bond failure, respectively.

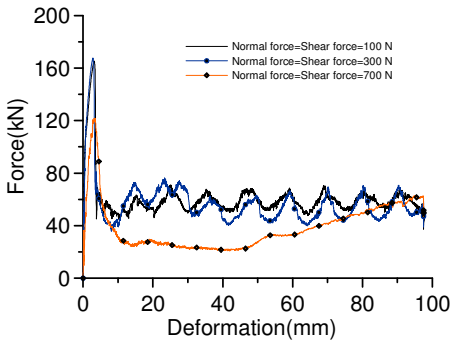

Fig. 3 Effect of adhesive failure limits on the force-displacement response of two-layered hybrid tubes

B. Mechanical Characteristics of Material

The metal tubes in this study were made of high-strength steel, which is a strain rate-sensitive material with a Young's modulus 195GPa, density 7850$kg/m^3$and yield stress 495MPa. To yield accurate numerical results, the stress-strain curves for various strain rates that were used in the numerical simulation. They were obtained by performing dynamic tensile tests using a Hopkinson Split Bar. Table 1 presents the mechanical properties of the composite tube, which were taken from the literatures proposed by Huang et al. (2009) and Hage et al. (2004).

TABLE I
MECHANICAL PROPERTIES OF UNIDIRECTIONAL CARBON/BMI RESIN LAMINA AND E-GLASS/EPOXY

Properity	Description	Value(Carbon)	Value(Glass)
ρ	Density	1.53 g/cm^3	1.80 g/cm^3
E_a	Longitudinal modulus (fiber direction)	135 Gpa	30.9 Gpa
E_b	Transverse modulus (perpendicular to fiber)	9.12 Gpa	8.3 Gpa
G_{ab}	In-plane shear modulus (ab plane)	5.67 Gpa	2.8 Gpa
v_{ba}	Minor poisson's ratio	0.021	0.0866
X_t	Longitudinal tension strength (fiber direction)	2326 Mpa	798 Mpa
X_c	Longitudinal compressive strength (fiber direction)	1236 Mpa	480 Mpa
Y_t	Transverse tension strength (perpendicular to fiber)	51 Mpa	40 Mpa
Y_c	Transverse compressive strength (perpendicular to fiber)	209 Mpa	140 Mpa
S_c	In-plane shear strength	87.9 Mpa	70 Mpa

C. Failure Criteria for Composite Layers

Composite material model 54 of LS-DYNA that was selected for our analysis was the most effective model of the composite material. That can input arbitrary properties of the orthotropic materials, and unidirectional layers in composite shell structures can be defined. Either the Tsai-Wu failure criteria or the Chang-Chang failure criteria for each lamina can be applied. The Chang-Chang failure criteria modified the Hashin's failure criteria to account for the non-linear shear stress-strain behavior, and the post-failure degradation was defined, enabling the behavior of the laminate to be analyzed after the failure of each successive lamina.

IV. RESULTS AND DISCUSSION

A number of indicators of crashworthiness are typically determined for crush components to evaluate their performance and compare it with that of other energy absorbing systems. The mean crushing force (P_m) and mass-specific energy absorption (E_s) are the primary parameters selected to evaluate the energy that can be absorbed by hybrid tubes. Generally, collapse involves plastic buckling and the formation of progressive folds. The formation of these folds causes the characteristic fluctuation in the axial force. Therefore, the mean crushing force in this investigation was defined as the average of the axial crushing force following the peak force (Fig. 4), and the mass-specific energy absorption is defined as,

$$E_s = \frac{E_{total}}{\Delta M} = \frac{E}{A\Delta L\rho} \tag{19}$$

where ΔM denotes the mass in the crushing length of the cylindrical tube; E_{total} is the total energy that is absorbed in the crushing process; ΔL represents the effective crushing length; ρ is density, and A is the cross-sectional area of the cylindrical tube.

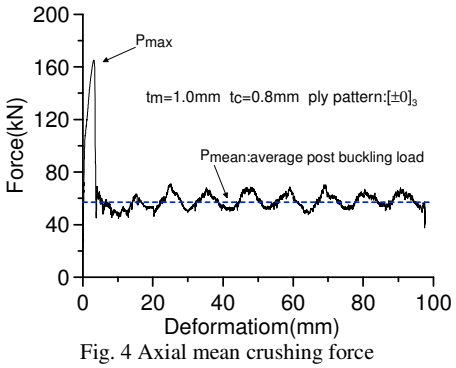

Fig. 4 Axial mean crushing force

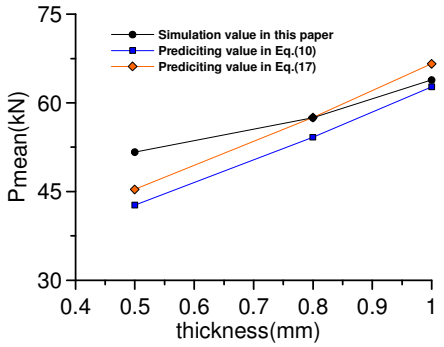

Fig. 5 Comparison between numerical simulation and analytical values of P_m calculated from Eq.(10) and (17)

TABLE II
COMPARISON BETWEEN SIMULATION RESULTS AND THE THEORETICAL PREDICTION VALUES FROM EQ (10) AND (17)

t_c (mm)	Simulation value of P_m	Predicting value of P_m from eq. (10)	Predicting value of P_m from eq. (17)	Error between equation (10) and simulation value	Error between equation (17)]and simulation value
0.5	51.70	42.74	45.38	17.33	12.22
0.8	57.50	54.22	57.56	5.70	0.10
1	63.90	62.74	66.64	1.82	4.29

A. Comparison with Previous Analytical Models

Cylindrical metal tubes that are externally wrapped with composites with three thicknesses under static crushing were simulated and the material mechanical properties in table 1 were utilized to obtain the theoretical prediction using Eqs. (10) and (17). Figure 5 and Table 2 compare the numerical and analytical results. Figure 5 plots of mean force as a function of thickness of the composite. All of the predicted values in the work of Wang and Lu (2002) exceeded those of in the work of Hanefi and Wierzbicki (1996). The simulated values are closer to the predictions based on Eq. (17). The percentage error between the simulated and predicted results was highest when the composite wall had a thickness of 0.5mm, and declined as the thickness of the composite increased. Even though a thickness of 0.5 mm was associated with a large error, the mean force at thicknesses of 0.8 and 1.0 mm were simulated with satisfactory accuracy, and the predicted and simulated results matched accurately. This result demonstrates that the developed finite element model yields satisfactory approximations to the theoretically predicted values.

B. Influence of Wall Thickness and Loading Condition

The simulation results show in tables 3 and 4 and Figs.6~10. Figure 6 plots force-deformation cures, which reveal that oscillations are followed by a high initial peak load. Since composite has a high strength to weight ratio, the figure indicates that the application of the composite significantly increases the crushing load, and the fiber-reinforced metal tubes exhibit excellent crashworthy performance.

Composites of three thicknesses (0.5, 0.8, 1.0 mm) were used to overwrap the steel tubes to form hybrid tubes. Figures 7 and 8 present the modeled results, which reveal that composite overwraps can be applied to enhance effectively the crushing characteristics and energy absorbing capacity of the tubes. As expected, increasing the thickness of the composite increased the mean crushing force. The mean crushing loads of the hybrid tubes were approximately 22.39, 44.53 and 62.69% higher than the corresponding values for the metal tubes, respectively (Fig.8). Figure 9 plots the crushing force against the crushing deformation. The dynamic and static results are identical in that they both reveal progressive failures, with only slight differences in the force-displacement curves. Comparing the static and dynamic crushing results demonstrates that although the folding patterns were very similar, increasing the impact velocity gives increased the force. Figure 10 indicates that the specific energy absorption increases with the thickness of the composite wall. Moreover, the figure shows that the responses in the static and dynamic tests were close to each other, for increasing the thickness. Apparently, the three composite wall thicknesses were insufficient to constrain the external movement of the metal tube. Therefore, the metal compound tube exhibited the properties of both steel and composite material. For this reason, the specific energy absorption increased gradually with a change in thickness of the composite.

TABLE III
SUMMARY OF CRUSHING CHARACTERISTICS OF METAL AND COMPOSITE COMPOUND TUBES UNDER STATIC LOADING

Description of model				Simulation results							
Material property	t_m (mm)	t_c (mm)	Ply pattern	Pmax (kN)	Pm (kN)	E_m (J)	E_c (J)	E_t (J)	E_s (J/kg)	Deformation (mm)	Energy increase(%
Bare mental	1.0	-	-	101.50	40.20	3967.80	-	3967.80	18.77	97.66	-
Carbon fiber	1.0	1.0	$[\pm0]_3$	174.60	65.40	5181.70	1125.20	6306.90	26.37	97.51	58.95
	1.0	0.8	$[\pm0]_3$	165.25	58.10	4978.50	847.26	5825.76	23.65	97.50	46.83
	1.0	0.5	$[\pm0]_3$	147.14	49.20	4684.10	491.96	5176.06	20.61	98.10	30.45
	1.0	0.8	$[\pm15]_3$	151.64	58.40	4877.20	935.33	5812.53	23.45	98.11	46.49
	1.0	0.8	$[\pm30]_3$	130.37	50.20	4004.20	948.51	4952.71	20.10	97.52	24.82
	1.0	0.8	$[\pm45]_3$	133.70	49.10	3726.90	1120.20	4847.10	19.58	98.00	22.16
	1.0	0.8	$[\pm60]_3$	137.28	53.50	3834.70	1403.90	5238.60	21.10	98.28	32.03
	1.0	0.8	$[\pm75]_3$	133.79	49.00	3871.50	939.90	4811.40	19.50	97.69	21.26
	1.0	0.8	$[\pm90]_3$	112.79	42.20	4031.10	128.44	4159.54	16.88	97.56	4.83
Glass fiber	1.0	0.8	$[\pm0]_3$	133.68	46.70	4111.90	524.02	4635.52	18.77	97.75	16.83
	1.0	0.8	$[\pm15]_3$	132.63	45.80	4085.60	534.67	4620.15	18.68	97.91	16.44
	1.0	0.8	$[\pm30]_3$	121.05	45.70	4023.20	587.87	4609.82	18.61	98.03	16.18
	1.0	0.8	$[\pm45]_3$	119.21	45.70	3932.80	634.63	4567.41	18.51	97.68	15.11
	1.0	0.8	$[\pm60]_3$	121.74	45.90	3873.10	691.93	4565.03	18.53	97.51	15.05
	1.0	0.8	$[\pm75]_3$	118.43	45.50	3974.40	619.12	4593.17	18.64	97.53	15.76
	1.0	0.8	$[\pm90]_3$	119.11	41.40	3984.40	190.03	4174.25	16.85	98.05	5.20

E_m and E_c represenr the energy absorption of metal and composite, respectively.
E_t is the total energy absorbed in the crushing process

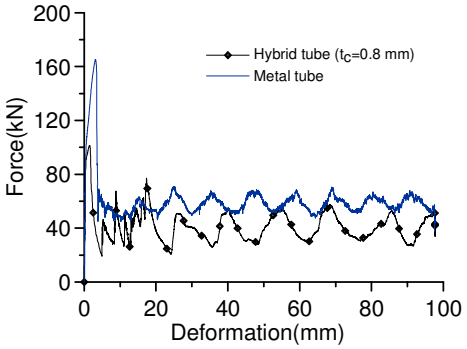

Fig. 6 Force-deformation curve of compound tube and bare metal tube subject to quasi-static crushing

TABLE IV
SUMMARY OF CRUSHING CHARACTERISTICS OF METAL AND CARBON COMPOSITE COMPOUND TUBES UNDER DYNAMIC LOADING

Description of model				Simulation results						
Loading condition	t_m (mm)	t_c (mm)	Ply pattern	Pmax (kN)	Pm (kN)	E_m(J)	E_c(J)	E_t(J)	E_s(J/kg)	Deformation(mm)
Dynamic (V=10 m/s)	1.0	-	-	103.14	44.30	5803.00	-	5803.00	19.78	135.55
	1.0	0.5	$[\pm0]_3$	154.61	56.60	5161.10	524.69	5685.79	22.28	99.70
	1.0	0.8	$[\pm0]_3$	172.37	59.70	4902.50	790.54	5693.04	24.89	90.52
	1.0	1	$[\pm0]_3$	180.71	63.10	4760.80	933.02	5693.82	27.22	85.29
	1.0	0.8	$[\pm15]_3$	156.98	54.10	4872.90	875.27	5748.17	22.78	99.86
	1.0	0.8	$[\pm30]_3$	138.17	51.10	4699.50	1086.80	5786.30	21.22	107.96
	1.0	0.8	$[\pm45]_3$	150.47	54.40	4489.20	1281.30	5770.50	21.17	107.92
	1.0	0.8	$[\pm60]_3$	177.73	56.90	4227.30	1496.20	5723.50	22.39	101.20
	1.0	0.8	$[\pm75]_3$	173.83	52.20	4627.20	1094.10	5787.50	20.95	108.11
	1.0	0.8	$[\pm90]_3$	184.36	45.30	5596.20	191.30	5693.04	18.09	126.65

E_m and E_c represenr the energy absorption of metal and composite, respectively.
E_t is the total energy absorbed in the crushing process

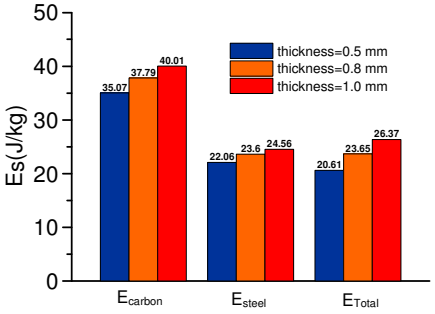

Fig. 7 Effect of thickness of composite on Es

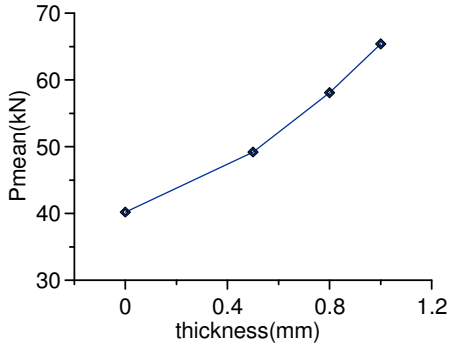

Fig. 8 Effect of composite wall thickness on P_m

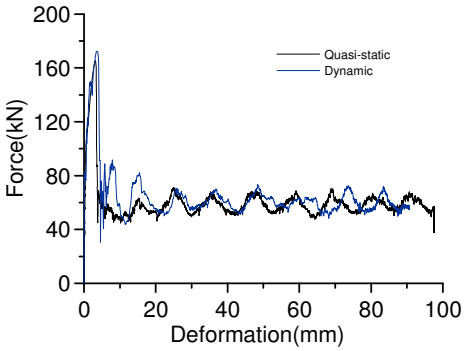

Fig. 9 Comparison of responses of force-deformation history curves to static and dynamic impacts

C. Effect of Ply Orientation

Figures11~14 present composites of a particular thickness (0.8mm) with different stacking sequences subject to quasi-static and dynamic crushing loading, to elucidate the

effect of the ply pattern on the energy absorption of the compund tubes.

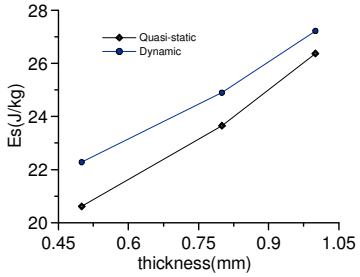

Fig. 10 Comparison of effect of composite wall thickness on energy absorption capacity in static tests with that in dynamic tests

Figure 11 indicates that the values of E_s and P_{mean} under dynamic loading exceed that under the quasi-static condition except when the ply orientation is $[\pm 15°]_3$. This result reveals that each ply is really not having a higher energy absorbing capacity under dynamic impact loading than under the quasi-static condition. Since the different ply patterns are associated with different energy absorption mechanisms of, as the winding angle increases to $[\pm 60°]_3$, the composite layer contributes increasingly to the energy absorption in the folding process and both loading conditions yields more similar results (Fig.12). However, even though the energy absorption capacity of the composite observably increases, the compound tube with the $[\pm 60°]_3$ ply pattern is really not the best energy absorber. In fact, the $[\pm 0°]_3$ compound tube exhibits the highest energy absorption capacity; although the contribution of its composite layer to that capacity is lower, because of the deformation mode. To study further the behavior of the hybrid tubes under axial deformation, Fig. 13 and Fig.14 plot their deformation profiles. As the winding angle exceeds 30, the concertina mode of the metal was replaced by a diamond mode. The energy efficiency in this axisymmetric mode is better than that of the asymmetric mode. Hence, as a side effect, the $[\pm 0°]_3$ compound tube has high energy absorption. When the metal tube exhibits an asymmetric collapse mode, the high energy absorption of the composite layer effectively results in a high energy absorption capacity of the hybrid tube. Accordingly, the energy efficiency of the composite plays an important role. The above analysis remarkably indicates that the energy absorption capacity depends strongly on the deformation mode of the metal tube and fiber-reinforcement does not affect the collapse failure mode of the metal. It also indicates that composite overwraps can effectively improve the crushing characteristics and energy absorbing.

D.Effect of Composite Property

Figure 15 illustrates the force-deformation curves of the carbon and glass fiber-reinforced metal tubes with $[\pm 0°]_3$ stacking orientation. The crushing responses of the compound tubes with 0.8 mm-thick carbon or glass composite demonstrate that the metal tube that is wrapped in carbon fiber enhances the crushing capacity a much more remarkably than that offered by the glass fiber. With respect to the first crushing force, the carbon fiber has the highest force-carrying capacity. However, the crushing force of the carbon fiber-reinforced metal tube also increases after the first peak crushing load is reached. Notably, the crushing force efficiency, defined as the ratio of the mean crushing load to the largest mean crushing load is 0.352 and 0.349 for the carbon and glass fiber, respectively. These values show that the hybrid tube with carbon fiber has a higher energy absorbing efficiency than the tube that is wrapped glass fiber.

Based on the results in Fig.16, neither fiber-reinforced metal tube exhibited a regular variation of the energy absorbing efficiency with the stacking orientation. The carbon fiber hybrid tubes produced a higher energy absorption capacity than the glass fiber for each ply pattern, whereas E_s of the glass fiber varies slightly with the ply pattern. In the case of $[\pm 90°]_3$, both materials respond similarly and substantially to variations in the ply pattern at $[\pm 0°]_3$ and $[\pm 15°]_3$. The $[\pm 0°]_3$ stacked fiber-reinforced metal tubes have the highest Es. As summarized in Table 3, carbon fiber improved the energy absorption capacity by 46.83%, whereas the glass fiber increased it by 16.83%. The results indicate that the compound tubes depend mainly on the tensile and compressive strength associated with the longitudinal and biaxial modulus of the materials. Accordingly, the selection of the composite material is important in ensuring favorable energy absorption capacity.

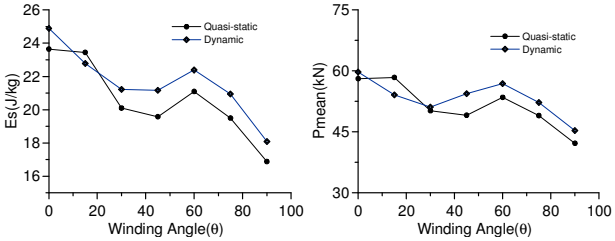

(a) (b)

Fig. 11 $[\pm\theta]_3$ stacked fiber-reinforced metal tubes (a)Energy absorption capacity (b) mean crushing force fiber-reinforced metal tubes

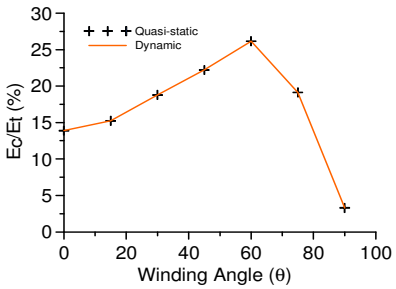

Fig. 12 Contribution of composite in $[\pm\theta]_3$ stacked fiber-reinforced metal tubes

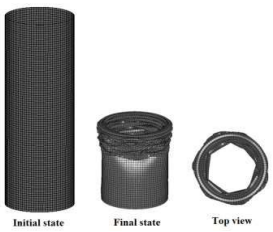

(a)

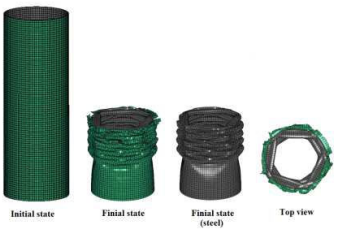

(b)

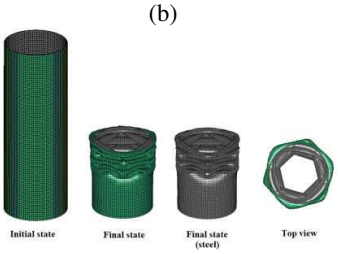

(c)

Fig. 13 Numerical models of deformation under static loading; (a) Metal tube, (b) Compound tube with $[\pm 0]_3$ ply pattern, (c) Compound tube with $[\pm 30]_3$ ply pattern

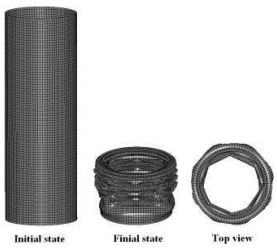

(a)

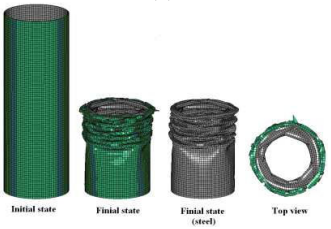

(b)

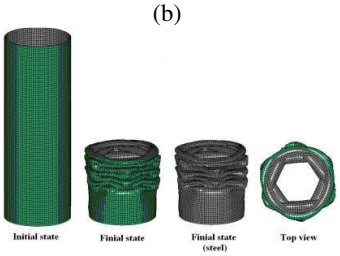

(c)

Fig. 14 Numerical models of deformation under dynamic loading; (a) Metal tube, (b) Compound tube with $[\pm 0]_3$ ply pattern, (c) Compound tube with $[\pm 30]_3$ ply pattern

V. Conclusion

The static and dynamic axial crushing behavior and energy absorption efficiency of metal tubes that are wrapped with composite were studied by including the effect of the strain rate on the metal layer. Overwrapping the metal tubes with composite is an effective means of increasing energy absorption capacity and the improving the crushing characteristics of such tubes. Energy absorption efficiency is examined as a function of composite wall thickness, loading condition, fiber ply orientation and composite property.

Simulations results are consistent with theoretical predictions. The results in this investigation reveal that the compound tubes undergo stable progressive failure in both quasi-static and dynamic crushing tests. A comparison of composites of various thicknesses demonstrates that the specific energy absorption in dynamic and static tests was an increasing function increased with the thickness of the composite wall. The stacking sequence significantly affects the energy absorption capacity. The $[\pm 0°]_3$ compound tube had the highest energy absorption efficiency of all tubes with the same thickness of composite. Notably, the collapse mode is an effective indicator of the energy absorption mechanism and the composite material property is also an important factor in determining energy absorption efficiency.

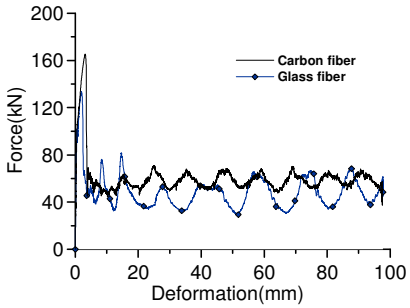

Fig. 15 Force-deformation curves of compound tubes that are wrapped with carbon and glass fibers with $[\pm 0°]_3$ ply pattern

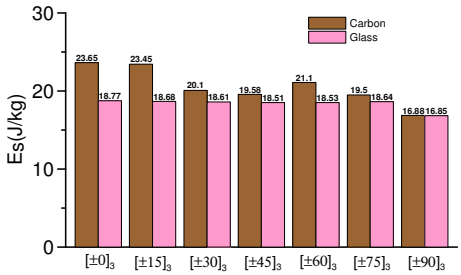

Fig. 17 Energy absorption capacities of compound tubes with various material properties of composite and stacking sequences, subject to quasi-static crushing

References

[1] Alexander JM. (1960),"An approximate analysis of the collapse of thin cylindrical shells under axial loading",The Quarterly Journal of Mechanics and Applied Mathematics., 13(1), 10-15.

[2] Abramowicz W (1983). "The effective crushing distance in axially compressed thin walled metal columns", Int. J. Impact Engng.,1(3), 309-317.

[3] Bambach MR (2010)."Axial capacity and crushing of thin-walled metal , fibre-epoxy and composite metal-fibre tubes", Thin Wall Struct;48(6), 440-452.

[4] Farley GL, Jones RM (1992),"Crushing characteristics of continuous fiber-reinforced composite tubes", J Compos Mater., 26(1), 37-50.

[5] Guillow SR, Lu G, Grzebieta RH (2001)," Quasi-static axial compression of thin-walled circular aluminium tubes", International Journal of Mechanical Sciences., 43(9), 2103-2123.

[6] Hanefi, EH, Wierzbicki, T (1996),"Axial crush resistance and energy absorption of externally reinforced metal tubes" ,Composite Part B: Eng.,27(5), 387-394.

[7] Hage H.EI., Mallick P.K., Zamani N (2004),“ Numerical modeling of quasi-static axial crush of square aluminum-composite hybrid tubes”, Int J Crashworthiness., 9(6), 653-664.
[8] Han H, Taheri F, Pegg N, Lu Y(2007),“A numerical study on the axial crushing response of hybrid pultraded and ±45° braided tubes”,Compos Struct., 80(2), 253-264.
[9] Huang J, Wang X. (2009),“Numerical and experimental investigations on the axial crushing response of composite tubes”,Compos Struct.,91(2), 222-228.
[10] Ismail A.E, Ahmad A (2007).“Crushing behavior of pultruded composites”, J. Mekanikal ; 24, 15-31.
[11] Kadi Hany EI.(2007),“Predicting the Crushing Behavior of Axially Loaded Elliptical Composite Tubes Using Artificial Neural Networks”, Appl Compos Mater.,15, 273-285.
[12] Mamalis AG, Manolakos DE, Ioannidis MB, Kostazos PK, Papapostolou DP. (2002),“Axial collapse of hybrid square sandwich composite tubular components with corrugated core: numerical modelling”,Compos Struct., 58(4), 571-582.
[13] Mamalis AG, Manolakos DE, Ioannidis MB, Papapostolou DP.(2006),“ The static and dynamic axial collapse of CFRP square tubes: finite element modelling”, Compos Struct.,74(2), 213-225.
[14] McGregor Carla.J. ,Vaziri Reza. , Poursartip Anoush ,Xiao Xinran.(2007),“ Simulation of progressive damage development in braided composite tubes under axial compression”, Composites (Part A).,38, 2247-2259.
[15] Song H.W., Wan Z.M., Xie Z.M., Du X.W (2000),“Axial impact behavior and energy absorption efficiency of composite wrapped metal tubes”,Int J Impact Eng 24, 385-401.
[16] Wang X, Lu G.(2002),“ Axial crushing force of externally fibre-reinforced metal tubes”, Proc. IMechE J Mech. Eng Sci., 216(9),863-874.
[17] Marais S.T., Tait R.B., Cloete T.J., G.N. Nurick (2004),“Material testing at high strain rate using the split Hopkinson pressure bar”, Latin American Journal of Solids and Structures,1 ,319-339
[18] LS-DYNA Theoretical Manual (2006), V.971, Livermore Software Technology Corporation, Livermore, CA, USA.